Optical Engineering

SPIEDigitalLibrary.org/oe

Spectral model of optical scintillation for terrestrial free-space optical communication link design

Kyung-Hwan Kim
Takeshi Higashino
Katsutoshi Tsukamoto
Shozo Komaki
Kamugisha Kazaura
Mitsuji Matsumoto

Spectral model of optical scintillation for terrestrial free-space optical communication link design

Kyung-Hwan Kim
Takeshi Higashino
Katsutoshi Tsukamoto
Shozo Komaki
Osaka University
Department of Electrical
Electronic and Information Engineering
Graduate School of Engineering
2-1, Yamada-oka
Suita-shi, 565-0871, Japan
E-mail: kkh@roms.comm.eng.osaka-u.ac.jp

Kamugisha Kazaura
Mitsuji Matsumoto
Waseda University
GITI
1-3-10, Nishiwaseda
Shinjuku-ku, 169-0051, Japan

Abstract. Since a deep and long-term fading in optical intensity results in considerable burst errors in the data, a terrestrial free-space optical (FSO) system has to be designed with consideration of a frequency characteristic of optical scintillation to achieve high quality wireless services over the link. In designing a terrestrial FSO link, we had better design the system considering variations caused by some slow time-varying parameters. This paper proposes a Butterworth-type spectral model of optical scintillation to design a terrestrial FSO link, which enables us to estimate the power spectral density of optical scintillation in a current optical wireless channel when time zone and weather parameters, such as temperature and rainfall intensity, are given. The spectral parameters of optical scintillation, cut-off frequency, and spectral slope are estimated from the data obtained in the experiment, and then their dependencies on time zone, temperature, and rainfall intensity are examined. [DOI: 10.1117/1.3557487]

Subject terms: optical scintillation; intensity fluctuation; power spectral density; terrestrial free-space optical communication.

Paper 100751R received Sep. 18, 2010; revised manuscript received Jan. 29, 2011; accepted for publication Feb. 1, 2011; published online Mar. 25, 2011.

1 Introduction

Free-space optical (FSO) systems have been developed as alternative promising technology for fiber optic systems due to their advantageous characteristics, such as high transmission security, wireless connectivity, cost-effective and quick installation, and license-free operation.[1–4] The FSO link has to be designed to achieve high quality transmission under the condition that atmospheric turbulence leads to intensity fluctuations of received optical signal, referred as optical scintillation.

In designing a terrestrial FSO system, the frequency characteristic of optical scintillation is one of the most important factors. For example, in a terrestrial FSO link with high-speed digital data transmission up to several gigabites per second, a deep and long-term fading in optical intensity results in considerable burst errors in the data. In compensating the intensity fluctuations by using the automatic gain control (AGC) function of an optical amplifier at an optical receiver side, slower response speed of the AGC causes degradation in the link performance. Many previous works on such terrestrial FSO systems have focused on its design or performance evaluation.[5–8] Reference 5 analyzes the FSO link availability considering the atmospheric effects, Ref. 6 examines the FSO link performance related parameters through a field experiment, Ref. 7 developes an optical propagation loss model for radio on a free space optical (RoFSO) link and applies it to design the link, and Ref. 8 describes an experimental evaluation on simultaneous transmission of multiple RF signals over their developed RoFSO link. For the system evaluation or design in these researches, however, the intensity fluctuation strength such as the scintillation index or the refractive index structure constant C_n^2 has been considered, but any consideration on the frequency characteristic of optical scintillation has not been found.

Recent terrestrial FSO links, such as the RoFSO link, employ direct focus on a received optical beam into a core of single-mode fiber (SMF)[6–15] that is much smaller than the detected area of a photodetector. Therefore, the beam tracking system needs higher ability to track the beam's angle-of-arrival (AOA) in the FSO link. References 14 and 15 present an example of the power spectra of the arrival-of-angle fluctuation of a 1550 nm beam and the optical scintillation variations of an 800 nm beam, and describe the correlation between them above 100 Hz. They focus on the effective tracking and steering beam to the SMF for frequency above 100 Hz. Therefore, an estimation model of optical scintillation's spectrum, especially its cut-off frequency, is necessary to achieve an adequate capacity of AGC and beam tracking.

Many studies related on the power spectral density (PSD) of optical scintillation have been carried out. Reference 16 considers the temporal frequency spectrum of the amplitude of a plane wave propagating through atmosphere, and the asymptotic forms for the temporal frequency spectra for plane and spherical waves are developed in Refs. 17–19. From the formulas, it is found that the spectra for both waves depend on the wind velocity. References 17 and 18 also characterize a spectrum of optical scintillation by cut-off frequency, and figure out the ratio of the cut-off frequency value to wind velocity component vertical to the directions of optical propagations length of 1000 and 2000 m. In Ref. 20, the dependency of optical scintillation frequency characteristic on the wind velocity is also described. It quantifies the relationship between the cut-off frequency of optical scintillation and the wind velocity component vertical to the direction of an optical propagation in cases of some different path lengths and heights. References 21 and 22 derive general formulas for the temporal frequency

0091-3286/2011/$25.00 © 2011 SPIE

spectra of amplitude fluctuations for plane and spherical waves, and extend them to the beam wave case. Reference 22 also presents a spectral model using the average and the fluctuation of wind velocity and obtains the frequency spectral slope proportional to $f^{-8/3}$ for a plane wave. In Ref. 23, the standard frequency spectral slope is compared to each PSD of beacon power at the quadrant photodiode and the signal power into the SMF. In this reference, it is observed that the beacon PSD follows the $f^{-8/3}$ spectral slope, but it seems that signal PSD rather follows the $f^{-4/3}$ spectral slope.

Optical scintillation spectrum will vary directly with wind velocity change. The wind velocity varies for a relatively shorter period than other parameters such as temperature and rainfall intensity. On the other hand, the design of the link budget or the employed modulation formats of a terrestrial FSO system requires the consideration of the scintillation spectrum averaged over a long time scale comparable to a weather condition such as temperature or rainfall intensity rather than rapid change in the wind velocity.

This paper proposes a Butterworth-type spectral model of optical scintillation for design of a terrestrial FSO link. The proposed PSD is determined by simple two parameters of the cut-off frequency and the spectral slope. The parameters of optical scintillation spectrum, cut-off frequency, and spectral slope are estimated from the data measured in the experiment, and then their dependencies on time zone, temperature, and rainfall intensity are examined. The goal of our analysis is to find the influences of temperature, rainfall intensity, and time zone on the scintillation spectrum. We note that the effect of wind velocity is eliminated by averaging over a long time scale.

This paper is organized as follows. In Sec. 2, we describe the FSO experimental configuration for the investigation. In Sec. 3, we propose a Butterworth-type PSD as optical scintillation's PSD. We show that the PSD can be approximated with a Butterworth-type PSD through analyzing the fluctuations in received optical intensity, and estimate the cut-off frequency and the spectral slope determining the PSD. In Sec. 4, first we investigate the characteristics of the estimated cut-off frequency and spectral slope for different values of weather parameters such as temperature and rainfall intensity. Differences of their characteristics between daytime and nighttime are disussed. In Sec. 5, estimating performance of the proposed PSD model is evaluated, and this paper is concluded in Sec. 6.

2 Experimental Setup for Measuring Optical Intensity Fluctuation Caused by Scintillation

Figure 1 shows a FSO experimental setup at the Waseda University in Tokyo. The distance between the optical antenna Tx and Rx with their apertures of 10 cm and the beam divergence angle of 5 mrad is 1 km. Both of Tx and Rx antennas are located on the rooftop of 10 floor buildings. An optical beam with its wavelength of 785 nm is radiated from the optical Tx antenna, and received at the photodiode (PD). The output current, $i(t)$, is sampled with its sampling rate of 10 kHz over a period of 3 s and recorded in the PC after every 5 min intervals. A weather meter to measure temperature and rainfall intensity is also installed on the rooftop of one of the buildings.

We note that our experiment is included in the case described above since the aperture diameters are 10 cm, and $\sqrt{\lambda L} = \sqrt{785\times10^{-9}\times10^{3}} = 2.8$ cm in the experimental setup. According to Refs. 17 and 18, if an aperture diameter exceeds $\sqrt{\lambda L}$, where λ is the optical wavelength and L is the propagation length, the spectral density of the intensity fluctuation at the higher frequencies are weakened significantly.

3 Approximated PSD of Optical Scintillation with Butterworth-Type Transfer Function

3.1 *Butterworth-Type PSD as a Spectral Model of Optical Scintillation*

As a spectral model of optical scintillation, we propose Butterworth-type PSD, which is characterized by two spectral parameters, cut-off frequency and spectral slope. We estimate cut-off frequencies and spectral slopes of optical scintillation for different weather conditions through fitting the autocorrelation of the impulse response of Butterworth filter to the measured autocorrelation $\phi_{ii}(\tau).\phi_{ii}(\tau)$. The $\phi_{ii}(\tau)$ is derived by $\phi_{ii}(\tau) = \phi'_{ii}(\tau)/\phi'_{ii}(0)$, where $\phi'_{ii}(\tau)$ is the measured autocovariance of $i(t)$.

The power transfer function of Butterworth filter is given by

$$|B(f)|^2 = \frac{1}{1+(f/f_c)^{2N}}, \tag{1}$$

where f_c is cut-off frequency, and N is the slope order. In Sec. 3.2, we will show the power transfer function of Butterworth filter is similar to the shape of optical scintillation's spectrum, and it becomes a good approximating method for optical scintillation PSD.

The impulse response of the first, second, and third order Butterworth filter, $b(t)$, is, respectively, given by

$$b(t) = \begin{cases} 2\pi f_c e^{-2\pi f_c t} \; ; N = 1 \\ 2\sqrt{2}\pi f_c \sin(\sqrt{2}\pi f_c t) e^{-\sqrt{2}\pi f_c t} \; ; N = 2 \\ 2\pi f_c [e^{-2\pi f_c t} + \{\sin(\sqrt{3}\pi f_c t)/\sqrt{3} - \cos(\sqrt{3}\pi f_c t)\} e^{-\pi f_c t}] \; ; N = 3 \end{cases}, \tag{2}$$

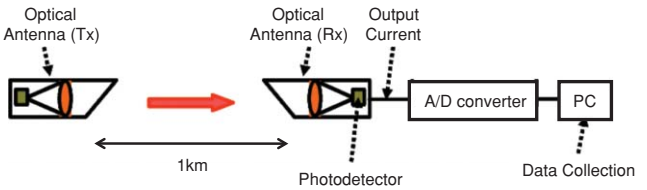

Fig. 1 Experimental setup.

where N is the slope order in higher frequency region. Furthermore, each normalized autocorrelation of $b(t)$, $\phi_{bb}(\tau)$, is obtained as

$$\phi_{bb}(\tau) = \frac{\int_{-\infty}^{\infty} b(t)b(t+\tau)dt}{\int_{-\infty}^{\infty} b^2(t)dt} = \begin{cases} e^{-2\pi f_c \tau} & N=1 \\ \sqrt{2}e^{-\sqrt{2}\pi f_c \tau}\sin(\sqrt{2}\pi f_c \tau + \pi/4) & ; N=2 \\ e^{-2\pi f_c \tau}/2 + \sin(\sqrt{3}\pi f_c \tau + \pi/6)e^{-\pi f_c \tau} & ; N=3 \end{cases} \tag{3}$$

We define $A_i(\tau)$ and $A_b(\tau)$ as the area under the curve of

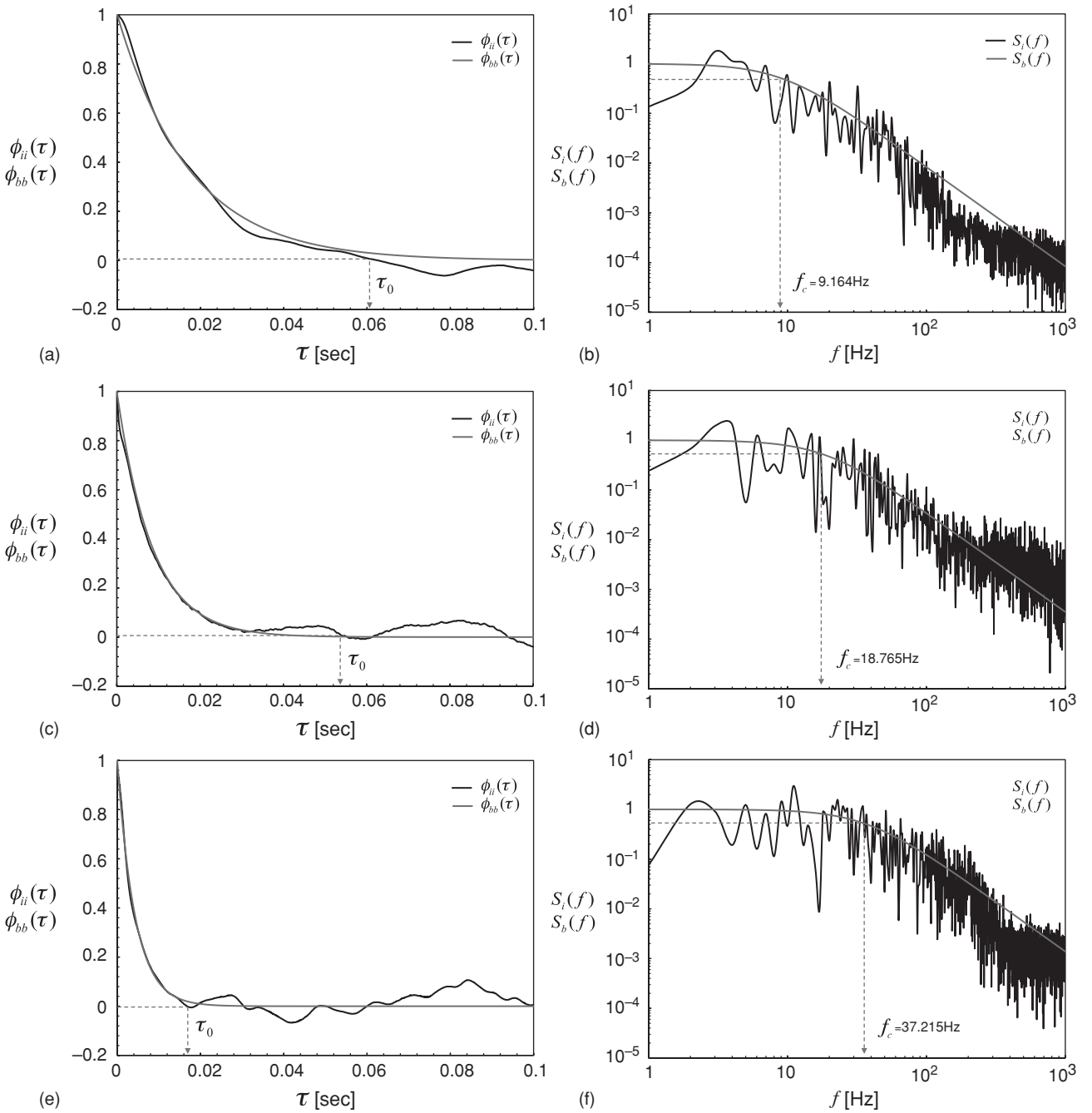

Fig. 2 (a) $\phi_{bb}(\tau)$ matched with $\phi_{ii}(\tau)$, and (b) $S_b(f)$ matched with $S_i(f)$.

Table 1 Each number of periods measured under combined weather conditions of θ and R.

	$\theta < 10$			$10 \leqq \theta < 20$			$20 \leqq \theta < 30$			$30 \leqq \theta$		
Number of Data	Daytime	Night	All day	Daytime	Night	All day	Daytime	Night	All day	Daytime	Night	All day
$R = 0$	1036	1675	4176	270	567	1192	3247	5494	13545	1682	181	2332
$0 < R \leqq 3$	837	758	2372	154	324	735	944	1377	3490	10	0	18
$3 < R \leqq 6$	8	9	29	16	37	73	68	159	323	1	0	1
$6 < R \leqq 9$	0	0	2	3	8	13	25	71	137	0	0	0
$9 < R$	0	0	0	3	12	17	35	60	115	1	0	1

$\phi_{ii}(\tau)$ and $\phi_{bb}(\tau)$, respectively,

$$A_i(\tau) = \int_0^{\tau} \phi_{ii}(\tau) d\tau$$
$$A_b(\tau) = \int_0^{\tau} \phi_{bb}(\tau) d\tau. \quad (4)$$

We derive a pair of approximated N and f_c satisfying the following equation,

$$A_i(\tau_0) = A_b(\tau_0), \quad (5)$$

in the sense of $\int_0^{\tau_0} \{\phi_{ii}(\tau) - \phi_{bb}(\tau)\}^2 d\tau = 0$, where τ_0 is the first zero-crossing time of $\phi_{ii}(\tau)$. Equation (5) means that the areas of the two waveforms of $\phi_{ii}(\tau)$ and $\phi_{bb}(\tau)$ are identical. In general, $\phi_{ii}(\tau)$ is small enough to disregard for a large τ. Figures 2(a), 2(c), and 2(d) show some examples of measured $\phi_{ii}(\tau)$ and $\phi_{bb}(\tau)$ satisfying Eq. (5). The approximated $\phi_{bb}(\tau)$ is obtained as follows. It is seen from these figures that the value of $\phi_{ii}(\tau)$ in $\tau > \tau_0$ becomes negligibly small. Therefore, we focus on high frequency components at a small τ, and find $\phi_{bb}(\tau)$ which fits to $\phi_{ii}(\tau)$ by making their areas identical within the integral range of $0 \leq \tau < \tau_0$. Each f_c for $N = 1$, 2, and 3 is respectively derived. Then, we select one of the autocorrelations to minimize the time averaged squared error, Δ, between the two waveforms of $\phi_{ii}(\tau)$ and $\phi_{bb}(\tau)$, where Δ is calculated by:

$$\Delta = \frac{1}{\tau_0} \int_0^{\tau_0} \{\phi_{ii}(\tau) - \phi_{bb}(\tau)\}^2 d\tau. \quad (6)$$

3.2 *Evaluation for the Approximating Performance*

Figures 2(a), 2(c), and 2(e) depict some examples of measured $\phi_{ii}(\tau)$ derived from experimental data and their approximations $\phi_{bb}(\tau)$. In the fitting, first, we calculate autocorrelation of normalized $i(t)$ by its mean value, $\phi_{ii}(\tau)$, from obtained data in the experiment as shown in Fig. 1. Then, we estimate cut-off frequency f_c and spectral slope N in the PSD by fitting $\phi_{bb}(\tau)$ to $\phi_{ii}(\tau)$ through the process as described in Sec. 3.1. It is observed that $\phi_{bb}(\tau)$ is well matched with $\phi_{ii}(\tau)$. Therefore, the power density spectra of $b(t)$, $S_b(f)$, are naturally matched with those of $i(t)$, $S_i(f)$, as plotted in Figs. 2(b), 2(d), and 2(f), respectively. For these samples, f_c of 9.164, 18.765, and 37.215 Hz are found, and N of 1 is found in all the cases. For these samples, Δ was 0.0004, 0.0004, and 0.0002, respectively.

An example of variations of measured temperature θ (°C), rainfall intensity R (mm/h), and f_c (Hz) over 24 h from 17 July 2006, 9:00 to 18 July 2006, 9:00 are shown in Fig. 3. Each point of f_c plotted in the graph in the figure denotes the f_c value obtained from each period of experimental data by the approximating process of optical scintillation's spectrum

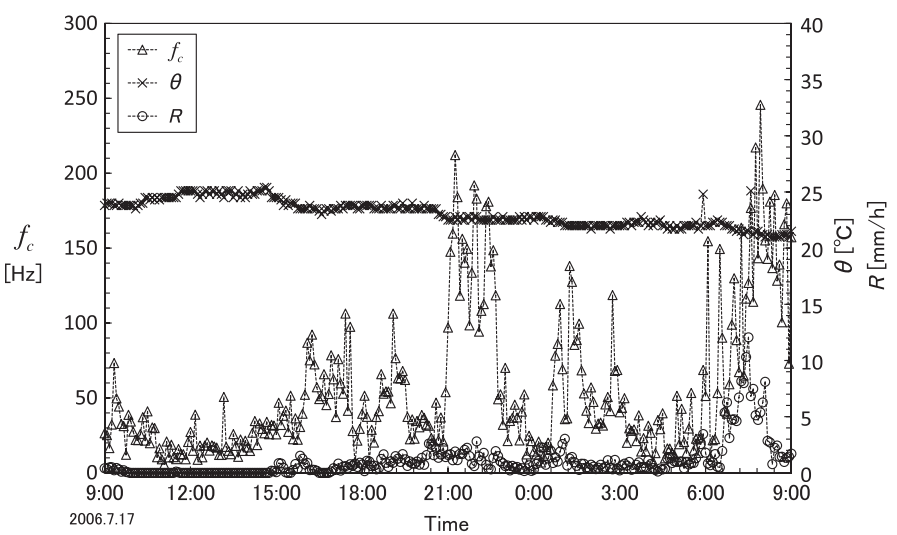

Fig. 3 An example of variations of temperature, rainfall intensity, and f_c during 24 h (2006. 7. 17 9:00 to 2006. 7.18 9:00).

Table 2 $\langle\Delta\rangle$ yielded by the approximating process by combined weather conditions of θ and R.

	$\theta < 10$			$10 \leqq \theta < 20$			$20 \leqq \theta < 30$			$30 \leqq \theta$		
$\langle\Delta\rangle$	Daytime	Night	All day	Daytime	Night	All day	Daytime	Night	All day	Daytime	Night	All day
$R = 0$	0.0046	0.0048	0.0049	0.0041	0.0038	0.0038	0.0036	0.0032	0.0034	0.0032	0.0032	0.0033
$0 < R \leqq 3$	0.0058	0.0072	0.0071	0.0064	0.0056	0.0057	0.0043	0.0067	0.0059	0.0047		0.0037
$3 < R \leqq 6$	0.0031	0.0134	0.0082	0.0071	0.0063	0.0065	0.0061	0.0117	0.0099	0.0031		0.0031
$6 < R \leqq 9$			0.0028	0.0155	0.01	0.0103	0.0066	0.0115	0.0091			
$9 < R$				0.0079	0.0146	0.0131	0.0056	0.0091	0.0074	0.0022		0.0022

described in Sec. 3.1. The total number of points is 288 in Fig. 3. In this manner, we have estimated spectral parameters of f_c and N corresponding to each period of FSO experimental data. As will be described in Sec. 4, we then will classify the obtained parameters by time zone and weather parameters such as temperature and rainfall intensity in order to model the optical scintillation's spectral parameters of f_c and N as their average value under given weather parameters. We summarized each number of periods under several combined weather conditions of θ and R used for our investigation in Table 1. The total number of periods corresponds to about 100 days.

Now, the performance of the approximating process is evaluated in terms of Δ by the weather conditions. We summarized average value of Δ, $\langle\Delta\rangle$, by combined weather conditions of θ and R in all day, daytime, and night in Table 2. The $\langle\Delta\rangle$ is defined by

$$\langle\Delta\rangle = \frac{1}{D}\sum_{j=1}^{D}\Delta_j, \tag{7}$$

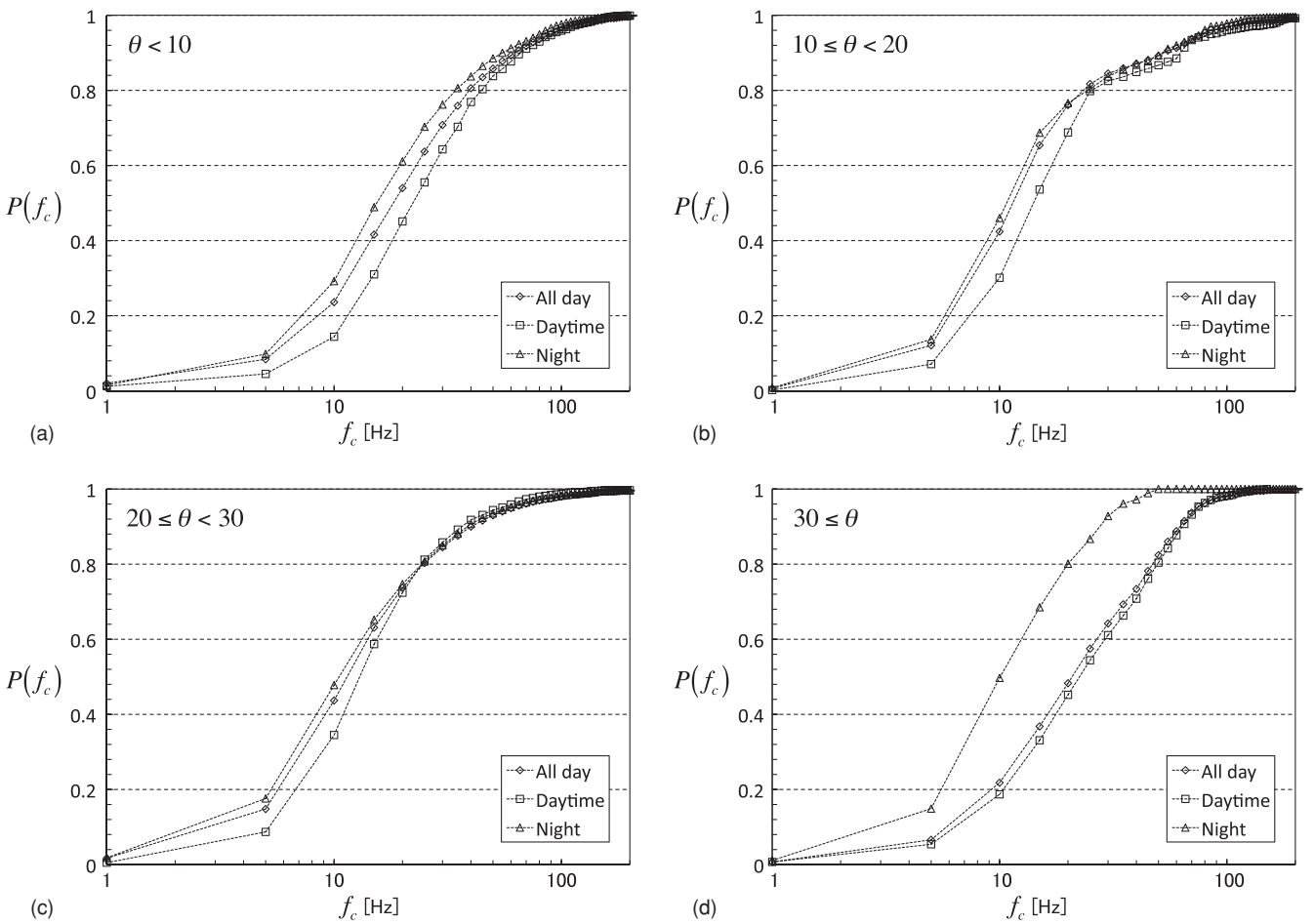

Fig. 4 $P(f_c)$ in each time zone: (a) for $\theta < 10$, (b) $10 \leqq \theta < 20$, (c) $20 \leqq \theta < 30$, and (d) $30 < \theta$.

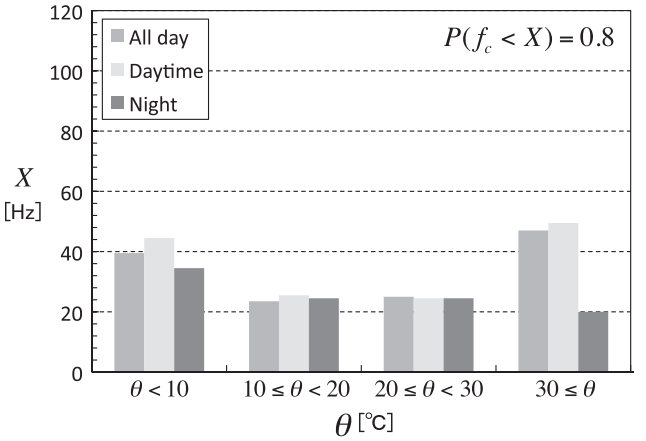

Fig. 5 X for θ in each time zone, where $P(f_c < X) = 0.8$.

where D denotes the total number of periods of data corresponding to combined weather parameters, and Δ_j is one of D number of Δ's. For example, there are $D = 4176$ periods of experimental data measured under the combined condition of $\theta < 10$ and $R = 10$ for the case of all days. Δ_j for each period of experimental data under the condition is calculated by Eq. (5), then their sum divided by 4176 is 0.0049. It is found that $\langle\Delta\rangle$ between $\phi_{ii}(\tau)$ and $\phi_{bb}(\tau)$ yielded by the process has the values from 0.0022 to 0.0155. The $\langle\Delta\rangle$ over all periods is 0.0044.

4 Dependency of f_c and N on Weather Parameters

If f_c and N can be estimated from some sort of conditions of a FSO link, we are able to estimate the PSD of optical scintillation that occurred in the link with Butterworth-type PSD. At that time, the characteristics of f_c and N depend on weather conditions, so their relationship among them is important.

In this section, with obtained f_c and N by using the approximating process described in Sec. 3, we quantify some values on the spectral shape of optical scintillation, $\langle f_c\rangle$ and $\langle N\rangle$, under weather conditions such as temperature θ (°C) and rainfall intensity R (mm/h), where $\langle f_c\rangle$ and $\langle N\rangle$ are averages of f_c and N, respectively. Differences of their values between daytimes (9:00–16:00) and night (0:00–4:00, 19:00–24:00), and their stats also are presented. On the basis of the results, we model the spectrum of optical scintillation.

Since there are a number of data in each identical condition of θ and R as shown in Table 1, the averaging period for measured data is enough long for the change of wind velocity. Therefore, it should be noted that the effect of wind is eliminated in the results presented in this paper.

4.1 *Dependency of f_c and N on Temperature*

Figures 4(a), 4(b), 4(c), and 4(d) show cumulative distribution functions of f_c and $P(f_c)$, for temperature conditions of $\theta < 10, 10 \leqq \theta < 20, 20 \leqq \theta < 30$, and $30 \leqq \theta$ in cases of daytime, night, and all day, respectively. We summarized each value of X for those conditions in Fig. 5, where $P(f_c < X) = 0.8$. While values of X for $\theta < 10$ and $30 \leqq \theta$ are relatively larger than those for the other range of θ at daytime, the value of X decreases as θ increases at night. The values of X at daytime are similar or more than those at night. Especially, the difference between the two cases is 29.5 Hz which is largest when $30 \leqq \theta$. If $\theta < 10$ or $30 \leqq \theta$ during the daytime, optical scintillation fluctuation is faster than in the other ranges of θ. However, optical scintillation has the slowest fluctuation when $30 \leqq \theta$ at night.

The tendency described above is also observed in Fig. 6(a). For the case of daytime, the values of $\langle f_c(\theta)\rangle$ for $\theta < 10$ and $30 \leqq \theta$ are about 33 Hz, which is the largest. At night, $\langle f_c\rangle$ decreases as temperature increases, and eventually $\langle f_c\rangle$ for $30 \leqq \theta$ is 15 Hz, which is the smallest among all cases shown in the graph. As described in Ref. 24, the spectrum of the refractive index fluctuations is proportional to the structure constant of the temperature fluctuations, C_T, and C_T is directly linked to the structure constant of the refractive index fluctuation, C_n^2. From this, we expect smaller amplitude and slower speed of scintillation as temperature fluctuations become lower. Although there are some pioneering studies on C_n^2 or C_T (Refs. 24 and 27), any discussion about their night behaviors have not been clarified. Meanwhile, Ref. 6 shows C_n^2 measured in summer and winter seasons, and we can observe that at night C_n^2 in summer is smaller than that in winter. From the result, we may estimate that C_T is relatively smaller in higher temperature at night, and thus $\langle f_c\rangle$ will be relatively small. For $30 \leqq \theta$, while $\langle f_c\rangle$ for the case of all day is very similar to that in case of daytime, there is a striking difference between two values of $\langle f_c\rangle$ for the cases of all day and night. It results from the difference

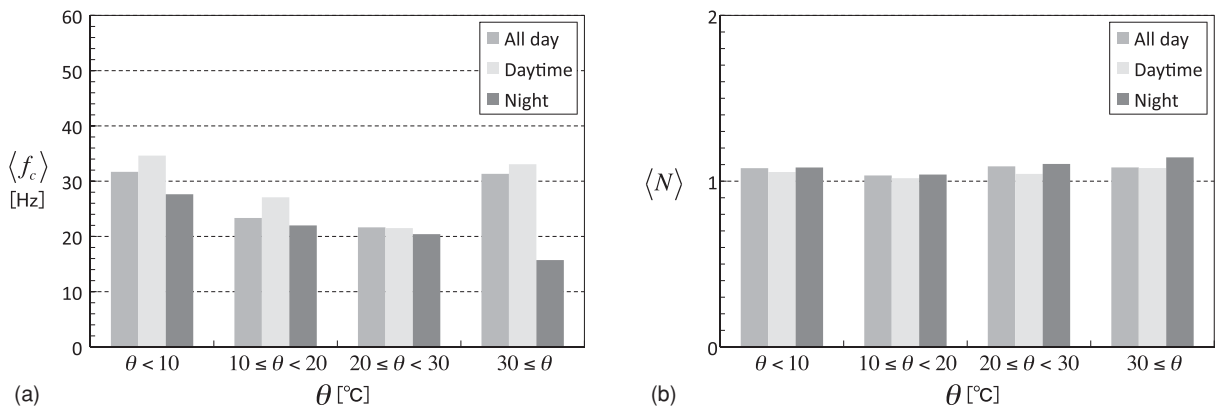

Fig. 6 (a) Each $\langle f_c\rangle$ and (b) $\langle N\rangle$ for θ in each time zone.

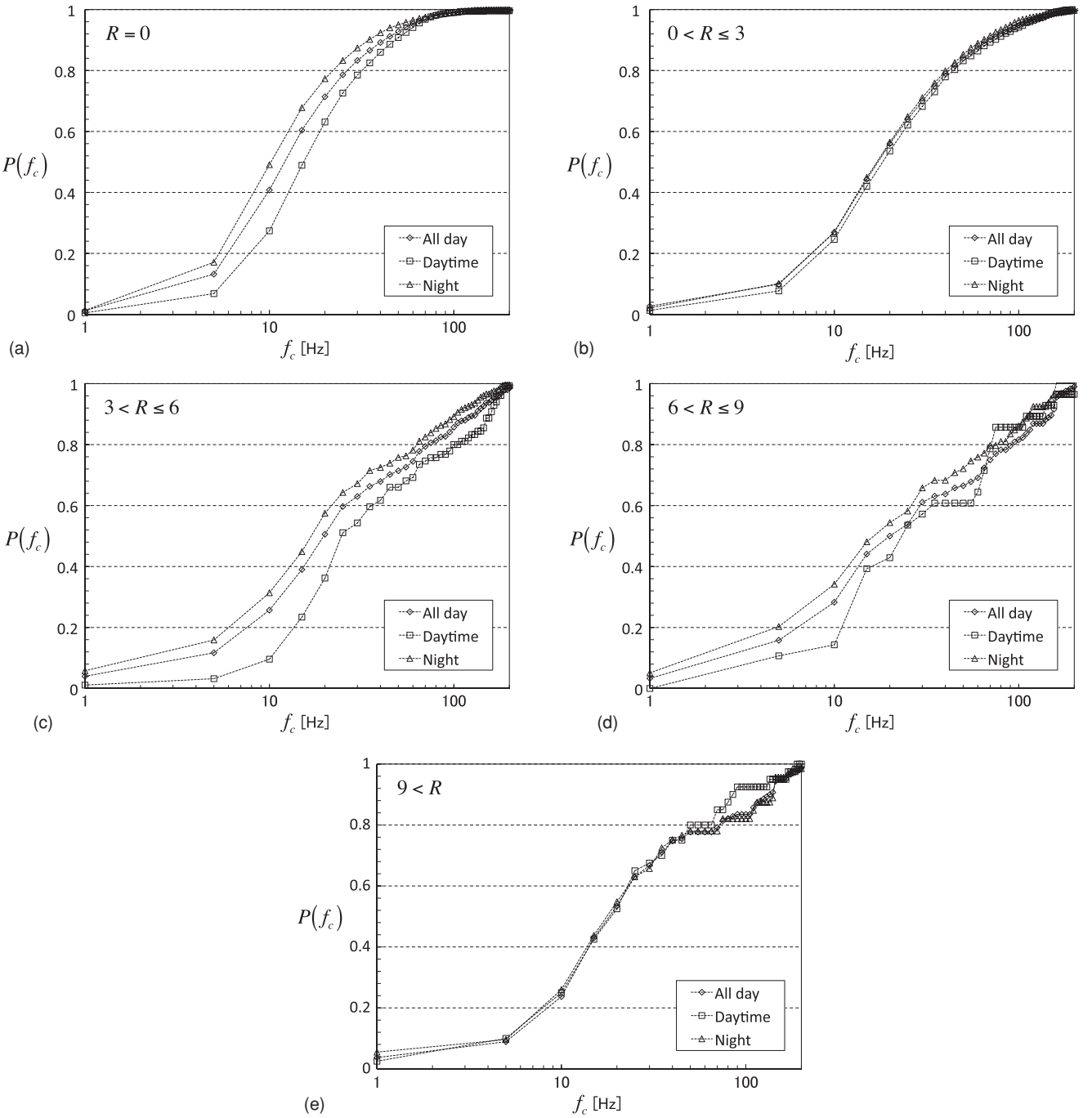

Fig. 7 $P(f_c)$ in each time zone (a) for $R = 0$, (b) $0 < R \leqq 3$, (c) $3 < R \leqq 6$, (d) $6 < R \leqq 9$, and (e) $9 < R$.

between the total number of periods for $30 \leqq \theta$ measured during the daytime and those at night, as the same reason mentioned above. For $30 \leqq \theta$, the tendency during the daytime dominates.

Figure 6(b) shows $\langle N \rangle$ for θ in cases of daytime, night, and all day. The value of $\langle N \rangle$ is almost constant as $\langle N \rangle \approx 1$ for all θ of any time zone. When $N = 1$ in Eq. (1), the spectral slope of optical scintillation is f^{-2} for high frequencies of $f \gg f_c$, and this result matches the conventional spectral model of $f^{-8/3}$ (Ref. 22).

4.2 *Dependency of f_c and N on Rainfall Intensity*

Figures 7(a)–7(b) show $P(f_c)$ for rainfall intensity conditions of $R = 0$, $0 < R \leqq 3$, $3 < R \leqq 6$, $6 < R \leqq 9$, and $9 < R$ for the cases of daytime, night, and all day, respectively. We summarized each value of X for those conditions in Fig. 8, where $P(f_c < X) = 0.8$. It is observed that X increases as R increases by a certain level of R for any time zone, and then X decreases as R increases when R exceeds that level. For the case of daytime, X increases up to 100.0 Hz as R increases by $3 < R \leqq 6$, it then begins decreasing when R

Table 3 Estimated values of f_c, $\hat{f}_c(\theta, R)$, under given combined weather conditions of θ and R.

	$\theta < 10$			$10 \leqq \theta < 20$			$20 \leqq \theta < 30$			$30 \leqq \theta$		
$\hat{f}_c$(Hz)	Daytime	Night	All day	Daytime	Night	All day	Daytime	Night	All day	Daytime	Night	All day
$R = 0$	28.2	24.1	25.6	26.6	18.8	19.9	18.5	17.0	18.6	33.1	15.7	31.4
$0 < R \leqq 3$	42.1	35.0	41.4	23.0	23.9	25.7	28.2	30.2	29.4	22.6		18.9
$3 < R \leqq 6$	82.5	66.9	97.1	76.9	56.9	58.8	50.8	33.1	40.1	34.8		34.8
$6 < R \leqq 9$			137.6	14.6	16.4	15.2	53.7	43.9	51.8			
$9 < R$				26.3	17.7	18.9	40.7	49.1	47.7	23.5		23.5

exceeds that range of R, and it reaches 65.0 Hz when $9 < R$. For the case of night, X increases up to 76.0 Hz as R increases by $6 < R \leqq 9$, and it seems that even though $9 < R$, without anymore outstanding increase or decrease, it becomes saturated as its value of 72.5 Hz, which is similar value to that for $6 < R \leqq 9$.

Each value of X in the case of daytime is larger than that in the case of night by $3 < R \leqq 6$, where the difference between them is 37.0 Hz, which is largest when $3 < R \leqq 6$. For $6 < R$, X at night becomes larger than that at daytime; there is difference of 5.0 to 7.5 Hz between them. X during a rainy period is larger than that during no rainy period for any time zone; the differences between them are 17.5 to 53.5 Hz at daytime, 12.5 to 68.0 Hz at night, and 16.0 to 64.5 Hz for the case of all day, respectively. In short, optical scintillation with no rainy period more slowly fluctuates than a rainy period.

For $0 < R \leqq 3$, $P(f_c)$'s in all cases of the time zone almost conforms to each other and there is also little difference among the values of X in three cases. Therefore, when $0 < R \leqq 3$, the value of X can be expected as that value in the case of all day regardless of time zone. For example, if the rainfall intensity condition of $0 < R \leqq 3$ is given only, we can expect the X of 42.5 Hz regardless of current time. In contrast, it is necessary to consider the time zone for $R = 0$ and $3 < R$.

The tendency described above is also observed in Fig. 9(a). In the case of daytime, $\langle f_c \rangle$ increases up to about 57.8 Hz as R increases by $3 < R \leqq 6$, it then begins to decreases when R exceeds that level, and it becomes about 39.2 Hz when $9 < R$. For the case of all day, $\langle f_c \rangle$ increases up to about 49.8 Hz as R increases by $6 < R \leqq 9$; it decreases up to 49.8 Hz when $9 < R$. For the case of night, however, $\langle f_c \rangle$ increases up to 57.8 Hz as R increases by $9 < R$ without decreasing, unlike the two cases of the time zone.

Figure 9(b) shows $\langle N \rangle$ for R for the cases of daytime, night, and all day. The value of $\langle N \rangle$ is almost constant as $\langle N \rangle \approx 1$ for all R of any time zone, as the result shown in Fig. 5(b). It is found that our result approximates to the conventional spectral slope of $f^{-8/3}$ also in the graph.

4.3 *Estimated Values of f_c and N Under Combined Conditions of Temperature and Rainfall Intensity*

We summarized the estimated value of cut-off frequency in the PSD of optical scintillation, $\hat{f}_c(\theta, R)$, under given combined weather conditions of θ and R for the cases of daytime, night, and all day in Table 3, where $\hat{f}_c(\theta, R)$ is defined as the average value of f_c under each combined condition, that is, $\hat{f}_c(\theta, R) = \langle f_c(\theta, R) \rangle$ in this paper. It should be noted that several blanks in the table do not denote zero, but that there is no data under the corresponding condition. The tendency of $\hat{f}_c$ corresponding to θ under condition of $R = 0$ agrees with results shown in Figs. 4, 5, and 6(a). However, there are some cases that disagree with such tendency under condition of $R \neq 0$. For example, for $3 < R \leqq 6$ in the case of all day, it is observed that $\hat{f}_c$ decreases as θ increases. When θ is only considered, the tendency of $\hat{f}_c$ corresponding to θ agrees with such tendency, because the number of data measured for each range of θ under condition of $R = 0$ is much

Table 4 *MSE* when the proposed model is applied to the design of a FSO link.

	$\theta < 10$			$10 \leqq \theta < 20$			$20 \leqq \theta < 30$			$30 \leqq \theta$		
MSE	Daytime	Night	All day	Daytime	Night	All day	Daytime	Night	All day	Daytime	Night	All day
$R = 0$	0.0159	0.0282	0.0238	0.0250	0.0308	0.0294	0.0156	0.0236	0.0242	0.0217	0.0151	0.0236
$0 < R \leqq 3$	0.0200	0.0226	0.0238	0.0203	0.0238	0.0262	0.0269	0.0256	0.0275	0.0089		0.0142
$3 < R \leqq 6$	0.0108	0.0175	0.0156	0.0223	0.0187	0.0235	0.0239	0.0270	0.0275	0.0031		0.0031
$6 < R \leqq 9$			0.0034	0.0169	0.0191	0.0178	0.0209	0.0209	0.0256			
$9 < R$				0.0103	0.0156	0.0148	0.0272	0.0236	0.0258	0.0022		0.0022

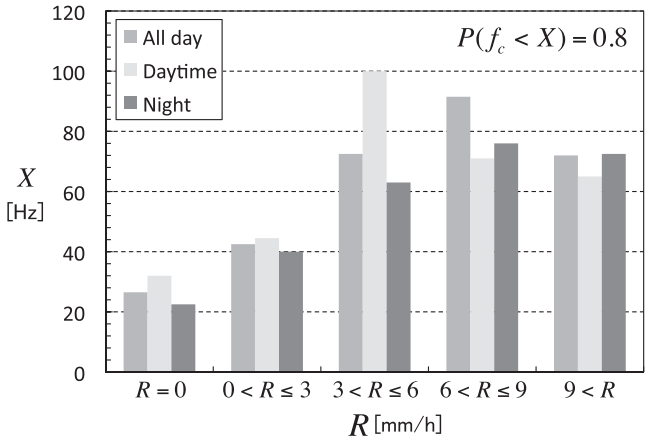

Fig. 8 X for R in each time zone, where $P(f_c < X) = 0.8$.

more than under the condition of $R \neq 0$. Especially, it was extremely rare for it to be $30 \leqq \theta$ while $R \neq 0$. Except for the cases of $10 \leqq \theta < 20$ at night and $30 \leqq \theta$, the tendency of $\hat{f}_c$ according to R agrees with results shown in Figs. 7, 8, and 9(a).

With regard to spectral slope, the estimated value of N is 1 which is denoted as $\hat{N} = 1$, regardless of θ and R, where $\hat{N}$ is defined as $\hat{N} = \langle N \rangle(\theta, R)$. In Secs. 4.1 and 4.2, we have observed that $\langle N \rangle$ is almost constant as $\langle N \rangle \approx 1$ in any ranges of θ and R of any time zone, and the result approximates to the conventional spectral slope of optical scintillation.

It should be noted that the proposed spectral model of optical scintillation is applicable in a FSO link with beam wavelength λ of 785 nm and beam propagation length L of 1 km. Since it is known that the cut-off frequency is in proportion to $1/\sqrt{\lambda L}$, we can estimate the cut-off frequency in a FSO link with arbitrary beam wavelength and propagation length if temperature and rainfall intensity are given only on the basis of Table 3. For example, for a FSO link with λ of 785 nm and L of 2 km, where $\sqrt{\lambda L} = \sqrt{785 \times 10^{-9} \times 2 \times 10^3}$, we may estimate the cut-off frequency under given conditions of temperature and rainfall intensity as $1/\sqrt{2}$ times the value of $\hat{f}_c$ corresponding to the condition in Table 3. Experimental confirmation with respect to the above will be further studied.

5 Estimating Performance of the Proposed Model

From our preceding discussion, we approximated PSD of optical scintillation by the proposed model of Butterworth-type PSD, and have collected the spectral parameters f_c and N from experimental data. We then classified the obtained parameters by time zone and weather parameters such as temperature and rainfall intensity, and model the estimated values of f_c and N as their average value under the given weather parameters and time zone. Therefore, if temperature and rainfall intensity are given, we are able to estimate PSD of optical scintillation in a current FSO link.

In this section, estimating the performance of the proposed model of optical scintillation's PSD is evaluated in terms of the mean square error (MSE) defined as following equation,

$$\mathrm{MSE} = \frac{1}{D} \sum_{k=1}^{D} \frac{1}{\tau_0^{(k)}} \int_0^{\tau_0^{(k)}} \{\hat{\phi}_{ii}(\tau; \hat{f}_c; \hat{N}) - \phi_{ii}^{(k)}(\tau; \theta; R)\}^2 d\tau, \tag{8}$$

where $\phi_{ii}^{(k)}(\tau; \theta; R)$ is one of $D - \phi_{ii}(\tau)$s in a same weather condition of θ and R, and $\tau_0^{(k)}$ is a zero-crossing time of $\phi_{ii}^{(k)}(\tau; \theta; R)$ at first. $\hat{\phi}_{ii}(\tau; \hat{f}_c; \hat{N})$ is an estimated autocorrelation for the given conditions, where $\hat{f}_c$ and $\hat{N}$ are determined by given θ and R. For example, when $\theta < 10$ and $R = 0$ in the daytime, $\hat{f}_c$ of 28.2 Hz and $\hat{N}$ of 1 are determined by Table 3, they are then substituted in Eq. (3); thus, $\hat{\phi}_{ii}(\tau; \hat{f}_c; \hat{N}) = e^{-56.4\pi\tau}$ in the condition. $\phi_{ii}^{(k)}(\tau; \theta; R)$ may change randomly due to variations of other weather parameters even in the same weather conditions of θ and R. Through calculating Eq. (6), we investigate the estimation error of $\hat{\phi}_{ii}(\tau; \hat{f}_c; \hat{N})$, a representative autocorrelation in a given condition θ and R, for variation of $\phi_{ii}(\tau; \theta; R)$.

We summarized the value of MSE for each combined weather parameters of θ and R in Table 4. It is found that MSE has a value between 0.01 and 0.03 on the whole. This table is one of the references when the estimation error is

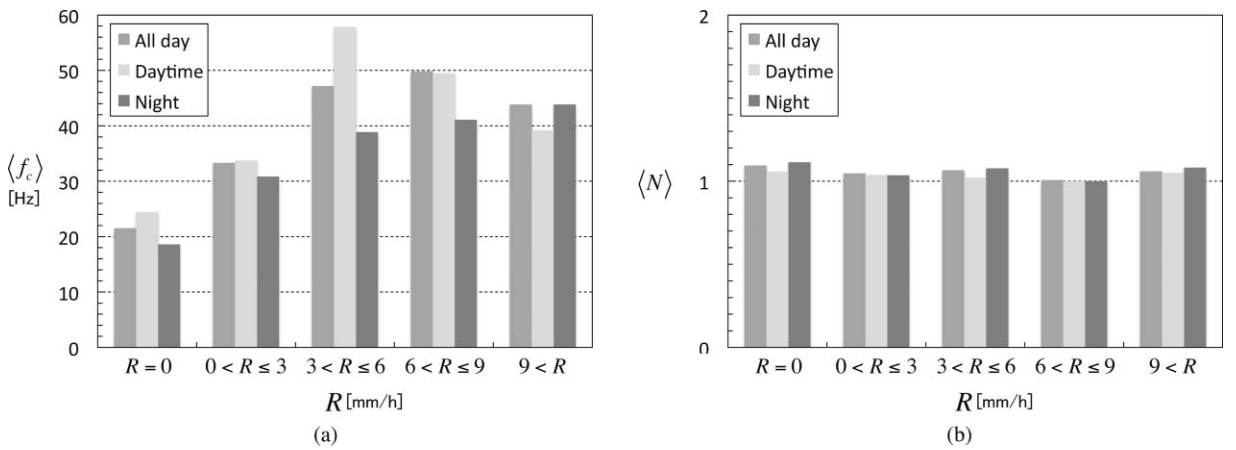

Fig. 9 (a) Each $\langle f_c \rangle$ and (b) $\langle N \rangle$ for R in each time zone.

restricted to be below a certain value in applying the proposed model to design a FSO link.

6 Conclusion

We have proposed the Butterworth-type PSD as optical scintillation's PSD for the design of a terrestrial FSO system. The spectral parameters of cut-off frequency and spectral slope, which determine the PSD, were estimated from the data measured in the experiment, and their dependencies on time zone, θ, and R were examined. The model enables us to estimate the PSD of optical scintillation in a FSO channel when such weather parameters are given.

The spectral model of optical scintillation is applicable for terrestrial FSO links with beam wavelength of 785 nm and beam propagation length of 1 km. In the case of FSO a link with a different beam wavelength or a different link length, however, we may estimate the PSD of optical scintillation by applying the relationship between cut-off frequency and $1/\sqrt{\lambda L}$ to the model for given weather conditions. This extension of the model should be experimentally confirmed, but due to the limitation in the experimental site, this confirmation will be further studied.

Acknowledgments

The experimental data were measured with experimental equipment developed in RoFSO project financially supported by the National Institute of Information and Communications Technology (NICT) of Japan, and we wish to express our appreciations.

References

1. H. Willebrand and B. Ghuman, *Free Space Optics: Enabling Optical Connectivity in Today's Networks*, Sams Publishing, Indianapolis, IN (2002).
2. D. Kedar and S. Arnon, "Urban optical wireless communication networks: the main challenges and possible solutions," *IEEE Optical Commun. Mag.* **42**, S2–S7 (2004).
3. V. W. S. Chan, "Free-space optical communications," *J. Lightwave Technol.* **24**(12), 4750–4762 (2006).
4. Report ITU-R F. 2106, "Fixed service applications using free-space optical links" ITU-R, Geneva, Swiss (2007).
5. A. Prokes, "Atmospheric effects on availability of free space optics systems," *Opt. Eng.* **48**(6), 066001-1-10 (2009).
6. P. T. Dat, A. M. Shah, K. Kazaura, K. Wakamori, T. Suzuki, K. Takahashi, M. Matsumoto, Y. Aburakawa, T. Nakamura, T. Higashino, K. Tsukamoto, and S. Komaki, "A study on transmission of RF signals over a turbulent free space optical link," *Proc. MWP*, 173–176 (2008).
7. K. Tsukamoto, T. Higashino, S. Komaki, K. Kazaura, K. Wakamori, T. Suzuki, and M. Matsumoto, "A new loss model and system design method for radio on free space optical link," *Proc. MWP*, 1–4, 2009.
8. A. Bekkali, P. T. Dat, K. Kazaura, K. Wakamori, M. Matsumoto, T. Higashino, K. Tsukamoto, and S. Komaki, "Performance evaluation of an advanced DWDM RoFSO system for transmitting multiple RF signals," *IEICE Trans. Fundamentals* **E92-A**(11), 2697–2705 (2009).
9. K. Tsukamoto, T. Higashino, T. Nakamura, K. Takahashi, Y. Aburakawa, S. Komaki, K. Wakamori, T. Suzuki, K. Kazaura, A. M. Shah, K. Omae, and M. Matsumoto, "Development of radio on free space optics system for ubiquitous wireless," *Proc. PIERS* **4**, 427–431 (2008).
10. K. Kazaura, K. Wakamori, M. Matsumoto, T. Higashino, K. Tsukamoto, and S. Komaki, "RoFSO: a universal platform for convergence of fiber and free-space optical communication networks," *IEEE Commun. Mag.* **48**(2), 130–137 (2010).
11. Y. Arimoto, M. Presi, V. Guarino, A. D'Errico, G. Contestabile, M. Matsumoto, and E. Ciaramella, "320 Gbit/s (8×40 Gbit/s) double-pass terrestrial free-space optical link transparently connected to optical fibre lines," *Proc. ECOC* 1–2 (2008).
12. E. Ciaramella, Y. Arimoto, G. Contestabile, M. Presi, A. D'Errico, V. Guarino, and M. Matsumoto, "1.28 terrabits/s (32×40 Gbits/s) WDM transmission system for free space optical communications," *IEEE J. Sel. Area. Comm.* **27**(9), 1639–1645 (2009).
13. K. Tsukamoto, A. Hashimoto, Y. Aburakawa, and M. Matsumoto, "The case for free space," *IEEE Microw. Mag.* **10**(5), 84–92 (2009).
14. K. Kazaura, K. Omae, T. Suzuki, M. Matsumoto, E. Mutafungwa, T. Murakami, K. Takahashi, H. Matsumoto, K. Wakamori, and Y. Arimoto, "Performance evaluation of next generation free-space optical communication system," *IEICE Trans. Electron.* **E90-C**(2), 381–388 (2007).
15. K. Kazaura, K. Omae, T. Suzuki, M. Matsumoto, E. Mutafungwa, T. O. Korhonen, T. Murakami, K. Takahashi, H. Matsumoto, K. Wakamori, and Y. Arimoto, "Enhancing performance of next generation FSO communication systems using soft computing-based predictions," *Opt. Express* **14**(12), 4958–4968 (2006).
16. R. S. Lawrence and J. W. Strohbehn, "A survey of clear-air propagation effects relevant to optical communications," *Proc. IEEE* **58**, 1523–1545 (1970).
17. V. I. Tatarskii, Wave Propagation in a Turbulent Medium, English transl., McGraw-Hill, NY, (1961).
18. V. I. Tatarskii, The Effects of the Turbulent Atmosphere on Wave Propagation, English transl., US. Dept. of Commerce, NTIS, Springfield, VA (1971).
19. S. F. Clifford, "Temporal-frequency spectra for a spherical wave propagating through atmospheric turbulence," *J. Opt. Soc. Am.* **61**(10), 1285–1292 (1971).
20. E. Ryznar, "Dependency of optical scintillation frequency on wind speed," *Appl. Opt.* **4**(11), 1416–1418 (1965).
21. A. Ishimaru, "Temporal frequency spectra of multifrequency waves in turbulent atmosphere," *IEEE Trans. AP* **AP-20**(1), 10–19 (1972).
22. A. Ishimaru, *Wave Propagation and Scattering in Random Media, Vol. 2*, IEEE Press, New York (1997).
23. Y. Arimoto, "Multi-gigabit free-space optical communication system with bidirectional beacon tracking," *IEEJ Trans. FM* **127**(7), 385–390 (2007).
24. V. Thiermann and A. Kohnle, "A simple model for the structure constant of temperature fluctuations in the lower atmosphere," *J. Phys.* **21**, S37–S40 (1988).
25. D. L. Hutt, "Modeling and measurements of atmospheric optical turbulence over land," *Opt. Eng.* **38**(8), 1288–1295 (1999).
26. S. N. Bendersky, N. Kopeika, and N. Blaunstein, "Atmospheric optical turbulence over land in middle east coastal environments: prediction modeling and measurements," *Appl. Opt.* **43** 4070–4079 (2004).
27. D. Sadot and N. S. Kopeika, "Forecasting optical turbulence strength on basis of macroscale meteorology and aerosols: Models and validation," *Opt. Eng.* **31**, 200–212 (1992).

Kyung-Hwan Kim received his BE degree in multimedia communication engineering from Kyung-Sung University, Busan, Korea in 2006, and his ME degree in communication engineering from Osaka University, Osaka, Japan in 2009. He is currently working toward his PhD degree at Osaka University, Osaka, Japan, engaging in research on radio and optical communication systems. He is a student member of IEICE. He was awarded the Best Student Paper Awards of IEICE and APMP, Japan and China in 2009, respectively.

Takeshi Higashino received his BE, ME, and PhD degrees in communications engineering from Osaka University, in 2001, 2002, and 2005, respectively. He is currently a research associate in the Department of Electrical, Electronic and Information Engineering at Osaka University, engaging in research on radio and optical communication systems.

Katsutoshi Tsukamoto received his BE, ME, and PhD degrees in communications engineering from Osaka University, in 1982, 1984, and 1995, respectively. He is currently an associate professor in the Department of Communications Engineering at Osaka University, engaging in research on radio and optical communication systems. He is a member of IEEE and ITE. He was awarded the Paper Award of IEICE, Japan in 1996.

Shozo Komaki received his BE, ME, and PhD degrees in electrical communication engineering from Osaka University, in 1970, 1972, and 1983, respectively. In 1972, he joined the NTT Radio Communication Labs., where he was engaged in repeater development for a 20-GHz digital radio system, 16-QAM, and 256-QAM systems. From 1990, he moved to Osaka University, Faculty of Engineering, and engaged in research on radio and optical communication systems. He is currently a professor of Osaka University. He is a senior member of IEEE, and a member of the Institute of Electronics and Information Communication Engineers of Japan (IEICE), and the Institute of Television Engineers of Japan (ITE). He was awarded the Paper Award and the Achievement Award of IEICE, Japan in 1977 and 1994, respectively.

Kamugisha Kazaura received his BEng (honors) degree in electronics and communications engineering from the University of Bath, Bath, United Kingdom in 1995, and his MSc and PhD degrees in global information and telecommunication studies from Waseda University, Tokyo, Japan, in 2002 and 2007, respectively. He is a visiting researcher at the Research Institute for Science and Engineering (RISE) of Waseda University, Japan. He worked as a telecommunication engineer for the Tanzania Telecommunications Company Ltd. from 1996 to 2002. His research interests are in the field of fixed and mobile broadband wireless communications networks, and free-space optics systems. He is a member of IEICE, IET, and SPIE.

Mitsuji Matsumoto received his PhD degree from Waseda University, Tokyo, Japan, in 1994. He has been a professor at the graduate school of Global Information and Telecommunication Studies (GITS), Waseda University, Japan, since 2000. He worked at NTT Laboratories from 1970, where he was engaged in the research and development of terminal design for telematics and multimedia systems. In 1996 he joined the faculty of Science and Engineering of Waseda University as a professor. He was a visiting professor at the Center of Excellence for Information and Communication Engineering, Scuola Superiore Sant'Anna, Italy, in 2008. In 2001 to 2004 he was vice chairman of ITU-T Study Group 16, responsible for studies related to multimedia services. His current research is on the engineering design for the next-generation wireless communication systems using infrared, visible light, and radio waves. He is a member of IEEE (SM'10), IET, and IEICE, IPSJ, IIEEJ in Japan.